Experimental study of the isovector giant dipole resonance in ^{80}Zr and ^{81}Rb

S. Ceruti,[1,2,3] F. Camera,[1,2] A. Bracco,[1,2] A. Mentana,[1,2] R. Avigo,[1,2] G. Benzoni,[2] N. Blasi,[2] G. Bocchi,[1,2] S. Bottoni,[1,2] S. Brambilla,[2] F. C. L. Crespi,[1,2] A. Giaz,[2] S. Leoni,[1,2] B. Million,[2] A. I. Morales,[1,2] R. Nicolini,[1,2] L. Pellegri,[1,2] S. Riboldi,[1,2] O. Wieland,[2] D. Bazzacco,[4] M. Ciemala,[5] E. Farnea,[4] A. Gottardo,[6,7] M. Kmiecik,[5] A. Maj,[5] D. Mengoni,[4,6] C. Michelagnoli,[4,6] V. Modamio,[7] D. Montanari,[4,6] D. Napoli,[7] F. Recchia,[4,6] E. Sahin,[7,8] C. Ur,[4] J. J. Valiente-Dobón,[7] B. Wasilewska,[5] and M. Zieblinski[5]

[1]*Dipartimento di Fisica dell'Università degli Studi di Milano, I-20133 Milano, Italy*

[2]*INFN, Sezione di Milano, I-20133 Milano, Italy*

[3]*KU Leuven, Instituut voor Kern- en Stralingsfysica, B-3001 Leuven, Belgium*

[4]*INFN, Sezione di Padova, I-35131 Padova, Italy*

[5]*Institute of Nuclear Physics, Polish Academy of Sciences, 31-342 Krakow, Poland*

[6]*Dipartimento di Fisica dell'Università degli Studi di Padova, I-35131 Padova, Italy*

[7]*INFN, Laboratori Nazionali di Legnaro, Legnaro I-35020, Italy*

[8]*Department of Physics, University of Oslo, P.O. Box 1048 Blindern, N-0316 Oslo, Norway*

(Received 15 September 2016; published 12 January 2017)

The isovector giant dipole resonance (IVGDR) γ decay was measured in the compound nuclei ^{80}Zr and ^{81}Rb at an excitation energy of $E^* = 54$ MeV. The fusion reaction ^{40}Ca + ^{40}Ca at $E_{\rm beam} = 136$ MeV was used to form the compound nucleus ^{80}Zr, while the reaction ^{37}Cl + ^{44}Ca at $E_{\rm beam} = 95$ MeV was used to form the compound nucleus ^{81}Rb at the same excitation energy. The IVGDR parameters extracted from the analysis were compared with the ones found at higher excitation energy ($E^* = 83$ MeV). The comparison allows one to observe two different nuclear mechanisms: (i) the IVGDR intrinsic width remains constant with the excitation energy in the nucleus ^{81}Rb; (ii) the isospin-violating spreading width (i.e., *Coulomb spreading width*) remains constant with the excitation energy in the nucleus ^{80}Zr. The experimental setup used for the γ-ray detection was composed by the AGATA demonstrator array coupled to the large-volume $LaBr_3$:Ce detectors of the HECTOR$^+$ array.

DOI: 10.1103/PhysRevC.95.014312

I. INTRODUCTION

Giant Resonances (GR) are nuclear excitation modes which play a key role in the study of nuclear structure for their connection with the bulk properties of nuclear matter [1]. The isovector giant dipole resonance (IVGDR), where protons oscillate against neutrons, is one of the strongly studied resonances in the past. Its centroid is related to the nuclear mass, the width is related to different damping mechanisms, and the strength exhausts the major part of the Thomas-Reiche-Kuhn energy-weighted sum rule for an electric dipole operator ($E1$ operator) [1–4].

In particular, the width of the resonance in the nuclear ground state can be described microscopically as a sum of three contributions, $\Gamma = \Gamma^{\uparrow} + \Gamma^{\downarrow} + \Gamma_{\rm frag}$, where $\Gamma^{\uparrow}$ is the escape width for particles evaporation, $\Gamma^{\downarrow}$ is the spreading width arising from the coupling with 2p-2h, 3p-3h,..., np $-$ nh configurations, and $\Gamma_{\rm frag}$ is the Landau damping. In medium-heavy nuclei the main contribution to the IVGDR width is due to $\Gamma^{\downarrow}$.

The possibility to build the IVGDR on excited states (as suggested by Brink [5] and Axel [6]) provides an excellent chance to obtain information on the nuclear structure in extreme conditions (high excitation energy, nuclear temperature, and angular momentum) [2]. However, the intrinsic structure of the resonance is not expected to change with the excitation energy because it depends only on the bulk properties of the nucleus.

The evolution of the IVGDR properties as a function of the excitation energy was intensively studied in several experiments and in nuclei in different mass regions. It was observed that, although the centroid of the resonance remains constant with the excitation energy, the width significantly increases with both the angular momentum and the nuclear temperature [7–14]. This can be explained by either assuming that the spreading width, $\Gamma^{\downarrow}$, increases with the excitation energy or assuming that the nucleus is characterized by an ensemble of deformations, giving rise to an increase of the total width of the resonance.

Indeed, to describe nuclear properties at finite temperature, one should take into account that the nucleus experiences a continuous range of deformations and space orientations because of quantum and thermal fluctuations [9,12,13]. As a consequence, the average deformation of the nucleus, $\langle\beta\rangle$, is nonzero even for nuclei without a deformed shape in the equilibrium [9]. A linear relation between $\langle\beta\rangle$ and the increase of the width of the resonance was proposed in Refs. [10,11]; furthermore, as the angular momentum increases, the nucleus tends to undergo oblate flattening due to centrifugal effects and the equilibrium deformation rapidly increases. The IVGDR strength function undergoes a further splitting, which causes an increase of the observed width.

The experimental results at intermediate temperature ($T \approx$ 1–2 MeV) were found to be in agreement with the theoretical calculations using the thermal-fluctuation model (TFM), which takes into account the variation of the nuclear shape as a function of the temperature and the angular momentum [12,13]. A key assumption of the model is that the intrinsic width, $\Gamma_{\rm int}$, considered as the width of the resonance in the ground state, is a constant of the system and it does not change with the excitation energy of the nucleus.

Additionally, the IVGDR can be exploited to test the validity of the isospin symmetry in self-conjugate nuclei. Indeed, in atomic nuclei, the presence of the Coulomb interaction between protons breaks this symmetry and induces a mixing between nuclear states with different isospin values (i.e., *isospin mixing*) [15]. As a consequence, a nuclear state results in an overlap of different isospin states [16,17]. The isospin-symmetry breaking can be observed through decays which would be inhibited by isospin selection rules. This is the case of the electric dipole transition (i.e., $E1$ transition) from self-conjugate nuclei in an $I = 0$ configuration [18–23]. Because the IVGDR exhausts the major part of the energy-weighted sum rule for an $E1$ transition, this resonance is a powerful tool to observe and quantify the isospin-mixing effects.

Wilkinson [24] and Morinaga [25] suggested that at high-excitation energy a partial restoration of the isospin symmetry occurs because of the very short lifetime of the nucleus that does not allow one to achieve a complete mixing. Harney, Richter, and Weidenmüller [26] proposed a theoretical framework to describe in a unique theory the competition between the Compound Nucleus (CN) decay and the isospin mixing induced by the Coulomb interaction. The latter quantity is governed by the isospin-violating spreading width, $\Gamma_C^{\downarrow}$, the so-called Coulomb spreading width. An interesting open question is whether or not this quantity depends on the excitation energy of the system.

This work is intended to show that both the intrinsic quantities, $\Gamma_{\rm int}$ and $\Gamma_C^{\downarrow}$, are independent of the nuclear excitation energy. To support this idea a combined analysis of data obtained in the same experimental setup was made.

The measurement of the γ decay of the IVGDR in the compound nuclei ^{80}Zr and ^{81}Rb at an excitation energy of $E^* = 54$ MeV is reported. The ^{80}Zr nucleus was formed in the symmetric fusion reaction ^{40}Ca + ^{40}Ca at $E_{\rm beam} = 136$ MeV, while ^{81}Rb was formed in the reaction ^{37}Cl + ^{44}Ca at $E_{\rm beam} = 95$ MeV. The experiment was performed at the Laboratori Nazionali di Legnaro using an array of segmented high-purity germanium (HPGe) detectors and large volume $LaBr_3$:Ce detectors (AGATA-HECTOR$^+$ array).

It is anticipated that (i) the experimental data are in agreement with the assumption that the intrinsic width of the resonance remains constant, despite the observation that the IVGDR width increases with angular momentum in the nucleus ^{81}Rb, and (ii) the isospin-mixing phenomenon is governed by the Coulomb spreading width, which was found to remain constant as a function of the excitation energy in the nucleus ^{80}Zr. The latter result integrates our previous work reported in Ref. [23]. In addition, because the analysis was based on a statistical-model calculation, particular emphasis is given in this work to the test of the statistical-model calculations using the low-energy transitions measured with the AGATA demonstrator.

II. EXPERIMENT

A. Experimental setup

The experiment was performed at the Laboratori Nazionali di Legnaro (LNL), Italy. The experimental setup was composed by an array of segmented HPGe, the AGATA (Advanced GAmma Tracking Array) demonstrator [27], coupled to an array of large-volume $LaBr_3$:Ce detectors [28], called HECTOR$^+$. In this experiment the AGATA demonstrator consisted of four triple clusters of segmented HPGe detectors (detection efficiency at $E_\gamma = 1.173$ MeV $\epsilon_{\rm det} = 7\%$). The HECTOR$^+$ array consisted of six large-volume $LaBr_3$:Ce (3.5" × 8") detectors and a smaller one (3" × 3") (detection efficiency at $E_\gamma = 1.173$ MeV $\epsilon_{\rm det} = 5\%$). The trigger condition restricted the data taking to coincidence events between γ rays detected in AGATA and in HECTOR$^+$.

TABLE I. $E_{\rm beam}$ is the energy of the incoming beam, $I_{\rm beam}$ is the average beam current, t is the target thickness, $\sigma_{\rm fus}$ is the fusion cross section calculated with the CASCADE code [29].

Reaction	$E_{\rm beam}$ (MeV)	$I_{\rm beam}$ (pnA)	t (μg/cm^2)	$\sigma_{\rm fus}$ (mb)
^{40}Ca + ^{40}Ca	136	3.5	500	500
^{37}Cl + ^{44}Ca	95	3	500	250

In the first phase of the experiment, the ^{81}Rb nucleus was formed using a beam of ^{37}Cl ($E_{\rm beam} \approx 95$ MeV, $I_{\rm beam} \approx 3$ pnA) on a target of ^{44}Ca (0.5 mg/cm^2). The data taking was $\sim$ 70 hr long. In the second part of the experiment, the ^{80}Zr nucleus was formed using a beam of ^{40}Ca ($E_{\rm beam} \approx 136$ MeV, $I_{\rm beam} \approx 3.5$ pnA) on a target of ^{40}Ca (0.5 mg/cm^2). The data taking was $\sim$ 110 hr long. The ion beams were provided by the TANDEM linear-accelerator complex. In Table I the main features of both reactions are summarized.

To correctly compare the detected γ-ray spectrum and the simulated one, the latter must be folded with the response function of the detector. In Fig. 1, the solid curve represents the CN γ-ray decay obtained with a statistical-model calculation, performed with the CASCADE code [29], while the dashed curve was obtained after the response-function folding.

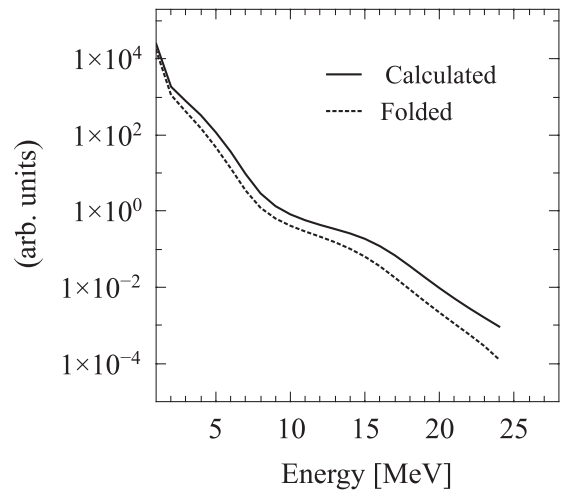

FIG. 1. CN γ-decay spectrum calculated with the CASCADE code before (solid line) and after (dashed line) the application of the detector response function.

The response function of the HECTOR$^+$ array was obtained by simulating the γ-ray interaction in the detectors starting from 1 MeV γ ray up to 32 MeV, obtaining 32 simulated spectra [30]. These spectra were considered as columns of a 32×32 matrix, where each element of the matrix ($E_{\rm det}$, E_γ) is the probability to detect a γ ray with $E_{\rm det}$ energy when a γ ray with an energy of E_γ interacts.

This matrix (called A) represents the response function of the detector. Indeed, if v is the incoming γ ray spectrum and w is the real detected spectrum, it is possible to write the relation

$$w = A * v, \tag{1}$$

where the symbol $*$ represents the vector product. The dashed curve in Fig. 1 was obtained using this procedure.

B. Angular-momentum distribution

In a fusion reaction, the CN spin distribution can be estimated by counting the number of γ rays emitted in the decay, the so-called γ-ray multiplicity (M_γ). M_γ is usually related with the CN spin J by the relation $J = 2M_\gamma + K$ [7], where K is the angular momentum removed by particle emission and statistical γ rays. In our case, the number of γ rays detected (the so-called γ-ray fold, F_γ) is always less than M_γ, because of the efficiency of the apparatus. Different F_γ values correspond to a different M_γ distribution and thus to a different CN angular-momentum distribution. Because the spin distribution is a fundamental input for the statistical model used in the analysis, it is important to know the conversion between F_γ and M_γ of the apparatus.

The relation between M_γ and F_γ was calculated using a simple recursive algorithm [31]. This algorithm calculates the probability $P(F_\gamma, M_\gamma)$ of measuring F_γ γ rays using N detectors and in a cascade of M_γ γ rays. As input, the experimentally predetermined total efficiency Ω of the apparatus and the intradetector scattering probability ξ are used:

$$\begin{aligned} P(F_\gamma, M_\gamma) = {} & a_F P(F_\gamma, M_\gamma - 1) \\ & + b_F P(F_\gamma - 1, M_\gamma - 1) \\ & + c_F P(F_\gamma - 2, M_\gamma - 1), \end{aligned} \tag{2}$$

with

$$\begin{aligned} a_F &= 1 - (N - F_\gamma)\omega\left(1 + \xi \frac{F_\gamma}{N-1}\right), \\ b_F &= (N - F_\gamma + 1)\omega\left(1 - \xi \frac{N - 2F_\gamma + 1}{N-1}\right), \\ c_F &= (N - F_\gamma + 2)\omega\xi \frac{N - F_\gamma + 1}{N-1}. \end{aligned} \tag{3}$$

$P(F_\gamma, M_\gamma) = 0$ for $F_\gamma < 0$ or $M_\gamma < 0$, and $P(0,0) = 0$. The efficiency of each detector of the apparatus is ω, i.e., $N\omega = \Omega$. In our case we neglected the scattering probability ξ, i.e., $\xi = 0$. $P(F_\gamma, M_\gamma)$ was calculated for a γ-ray energy of 1.173 MeV (γ transition coming from the ^{60}Co source). The $P(F_\gamma, M_\gamma)$ distributions are shown in Figs. 2 (for AGATA) and in Fig. 3 (for HECTOR$^+$). It should be noted that the granularities of the two detectors are very different: 12 HPGe detectors in AGATA and 7 detectors in HECTOR$^+$.

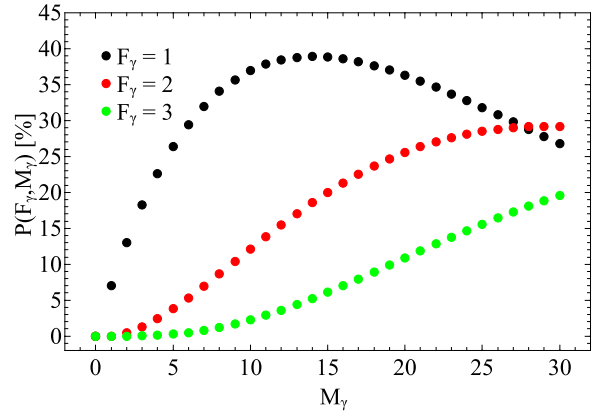

FIG. 2. Probability distribution $P(F_\gamma, M_\gamma)$ of triggering F_γ in the AGATA demonstrator by a cascade of M_γ γ rays. Three F_γ conditions are considered. A total efficiency $\epsilon_{\rm riv} = 7\%$ was considered in the calculations.

Because the detection of a γ ray in the AGATA demonstrator is statistically independent from the detection of another γ ray in HECTOR$^+$, the probability distribution $P(F_\gamma, M_\gamma)$ associated with a trigger condition corresponding to a coincidence between AGATA and HECTOR$^+$ was obtained by multiplying the $P(F_\gamma, M_\gamma)$ of the two detectors. The probability distributions for three different trigger conditions are shown in Fig. 4. To obtain the angular-momentum distribution related to a particular fold condition, the angular-momentum distribution obtained with CASCADE is folded with $P(F_\gamma, M_\gamma)$. The effect of the folding is shown in Fig. 5 for an event with $F_\gamma = 2$.

C. High-energy spectra

The high-energy γ rays emitted in the CN decay were detected by the HECTOR$^+$ array. The major part of the data was detected with a coincidence between HECTOR$^+$ and AGATA demonstrator. To reject background events, a gating condition on the time of the events was applied.

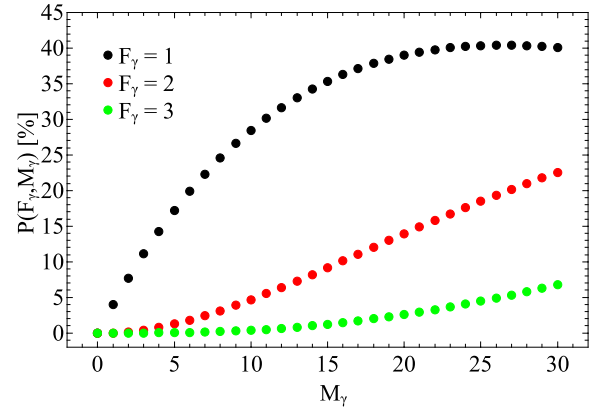

FIG. 3. The same as Fig. 2 but for the HECTOR$^+$ array. A total efficiency $\epsilon_{\rm riv} = 5\%$ was considered in the calculations.

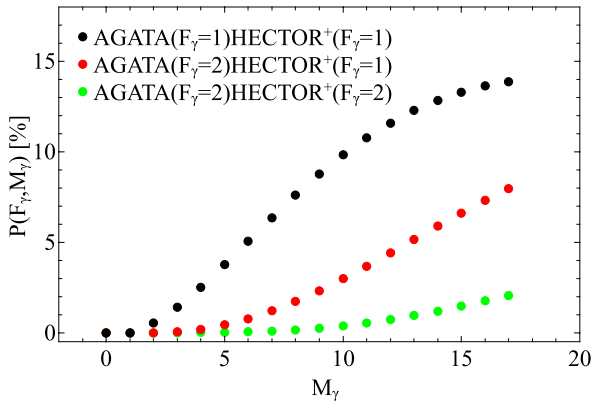

FIG. 4. The same as Fig. 2 but for different coincidence conditions between AGATA and HECTOR$^+$.

In Fig. 6, the γ-ray spectra detected in HECTOR$^+$ are shown. Despite the gating condition on the time of the events, the high-energy part of the spectrum exhibits a large background, which can be originated by nucleon-nucleon Bremsstrahlung or cosmic radiation. These high-energy γ rays interact with the neighboring material and the pair-production is the most probable reaction mechanism. Indeed, no γ-ray transitions were observed in the AGATA demonstrator in coincidence with $E_\gamma > 20$ MeV in HECTOR$^+$ and the only strong contribution comes from the 511 keV peak (see Fig. 7).

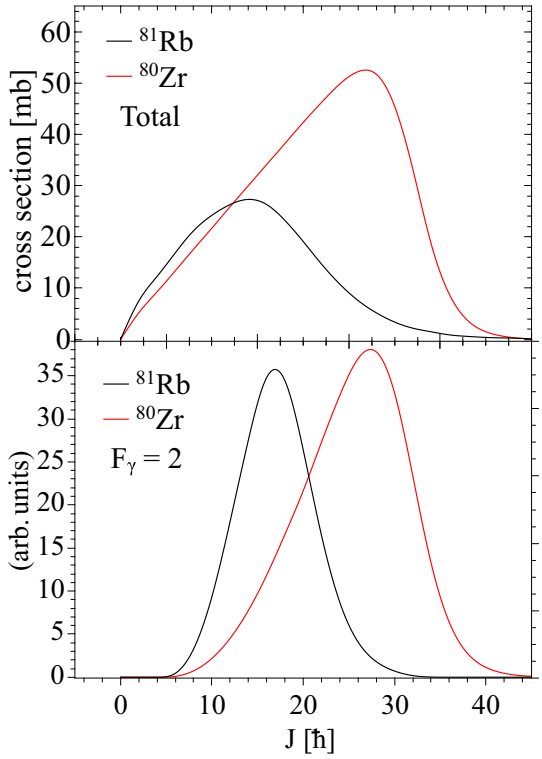

FIG. 5. Top panel: The angular-momentum distributions of the compound nuclei ^{80}Zr (red line) and ^{81}Rb (black line) calculated with the CASCADE code are shown. Bottom panel: Angular-momentum distributions folded with the response function for the coincidence $F_\gamma = 1$ in AGATA and $F_\gamma = 1$ in HECTOR$^+$ are shown.

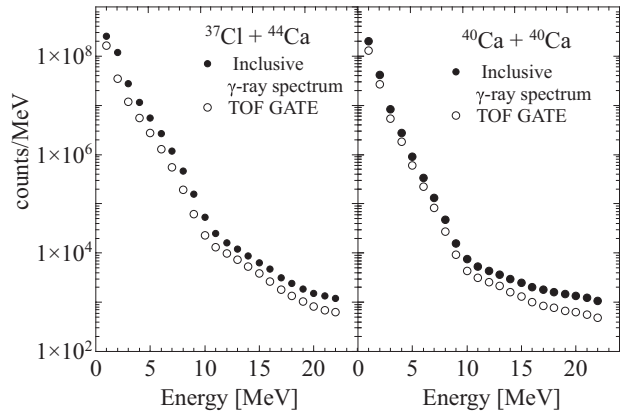

FIG. 6. Comparison between the inclusive γ-ray spectra (solid dots) and the time-gated γ-ray spectra (empty dots). The ^{37}Cl + ^{44}Ca spectra are plotted on the left, whereas the ^{40}Ca + ^{40}Ca spectra are plotted on the right.

Furthermore, observing the E_γ-E_γ matrix (energy detected in the AGATA demonstrator versus energy detected in HECTOR$^+$) shown in Fig. 8, it is evident that many events are characterized by the coincidence between two high-energy γ rays. In the CN decay, these kind of events are very unlikely, because, in general, only one high-energy γ ray is emitted in the decay process. In Fig. 9, the comparison between the HECTOR$^+$ spectrum in coincidence with a high-energy γ ray ($E_\gamma \geqslant 10$ MeV, region 2 in the matrix) and a low-energy γ ray ($E_\gamma \leqslant 4$ MeV, region 1 in the matrix) detected in AGATA is shown. As expected, the high-energy spectra in coincidence with another high-energy γ ray exhibit a flat shape and no resonance structure is visible. On the other hand, the other spectra exhibit a change in the slope at $\sim$10 MeV, typical of the presence of the IVGDR.

Because the background contribution in the high-energy part of the spectrum is similar in both reactions, the average of the spectra obtained in coincidence with a high-energy γ

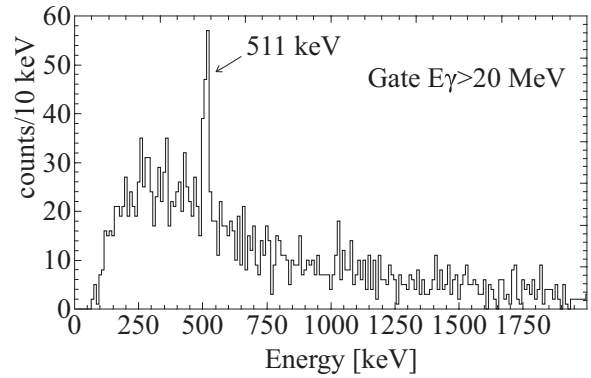

FIG. 7. Low-energy spectrum of the AGATA demonstrator in coincidence with a high-energy γ ray ($E_\gamma \geqslant 20$ MeV) detected in HECTOR$^+$. No transitions are visible and only the 511 keV peak is present.

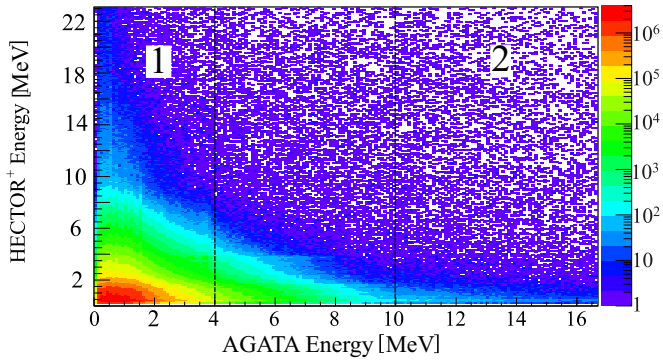

FIG. 8. E_γ-E_γ matrix for the reaction ^{40}Ca+^{40}Ca. On the x axis the energy detected in the AGATA demonstrator is plotted, whereas on the y axis the energy detected in HECTOR$^+$ is plotted. Two regions in the matrix are indicated: $E_\gamma \leqslant 4$ MeV (region 1) and $E_\gamma \geqslant 10$ MeV (region 2).

ray detected in AGATA was taken as the best estimation of the background. A linear function was used to fit the data in the high-energy part of the spectrum. The spectra obtained after a background subtraction (red dashed line) are shown with empty dots in Fig. 10. The typical IVGDR shape is clearly visible in the region between 10 and 20 MeV.

III. STATISTICAL-MODEL ANALYSIS

In the analysis a statistical-model approach is used to describe the CN decay. The statistical-model analysis was performed using the CASCADE code [29] in which the isospin formalism was also included.

The experimental method used to extract the isospin mixing is based on the assumption that the statistical-model parameters used to describe the IVGDR γ decay of ^{81}Rb and ^{80}Zr are the same (see Ref. [23] and references therein). The

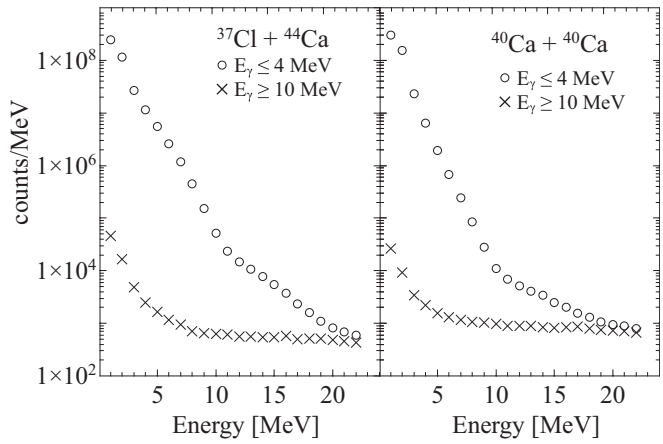

FIG. 9. Comparison between the γ-ray spectra obtained with two different conditions: $E_\gamma < 4$ MeV γ ray detected in AGATA (empty dots), $E_\gamma > 10$ MeV γ ray detected in AGATA (crosses). The ^{37}Cl+^{44}Ca spectra are plotted on the left, whereas the ^{40}Ca+^{40}Ca spectra are plotted on the right.

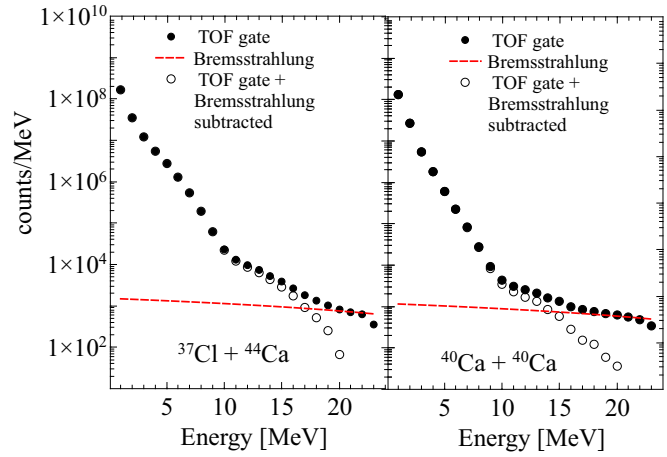

FIG. 10. Comparison between the time-of-flight (TOF) gated γ-ray spectrum (solid dots) and the γ-ray spectrum after the Bremsstrahlung subtraction (empty dots). The red dashed line is the estimated background contribution.

experimental key aspect to fulfill the previous assumption is that both ^{81}Rb and ^{80}Zr have a similar average CN temperature, mass, and angular-momentum distribution. In such a situation, as the IVGDR parameters depend on the bulk properties of the nucleus, one can assume the same set of parameters (centroid, width, and strength) to describe the statistical decay of the two nuclei. Table II shows that the kinematics of the reactions ensures the formation of the CN under a similar temperature and angular-momentum distributions. The average temperature of the CN was estimated as $\langle T\rangle = \sqrt{(E^* - \langle E_{\rm rot}\rangle - E_{\rm GDR})/a}$, where a is the level density parameter defined as $a = A/8$ MeV^{-1}.

If the properties of the statistical γ decay of the giant dipole resonance (GDR) could be extracted from the ^{81}Rb experimental data, the hindrance due to isospin mixing can be obtained from ^{80}Zr experimental spectra as a unique free parameter.

However, because our analysis was based on a statistical-model approach, it is mandatory to check if the model correctly reproduces the reaction mechanism. Therefore, an important step of the analysis was to check the agreement between the experimental data and the simulated ones. The physical observable used for this check is the distribution of the residual nuclei populated in the reaction.

TABLE II. Mean values of angular momentum $\langle J\rangle$, rotational energy $\langle E_{\rm rot}\rangle$, and temperature $\langle T\rangle$ are reported. The uncertainties were estimated using the standard deviation of the angular-momentum distribution.

CN	E^*(MeV)	$\langle J\rangle(\hbar)$	$\langle E_{\rm rot}\rangle$(MeV)	$\langle T\rangle$(MeV)
^{80}Zr	54	25 ± 6	14 ± 7	1.6 ± 0.3
^{81}Rb	54	17 ± 4	6 ± 3	1.8 ± 0.1

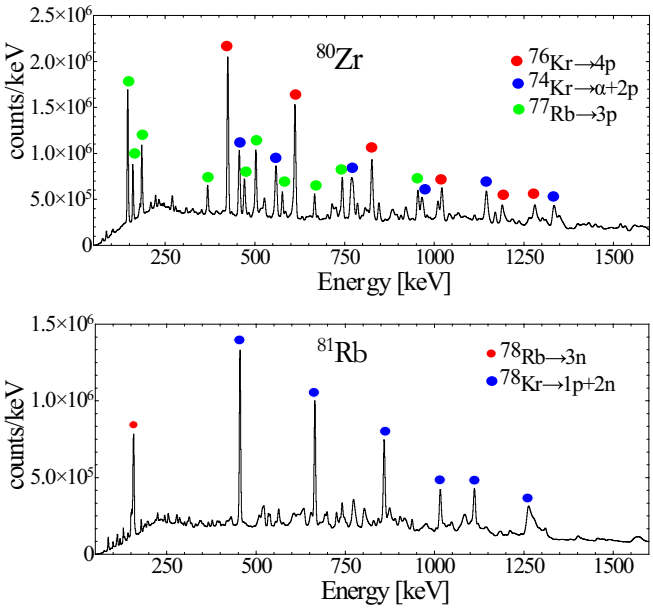

FIG. 11. The low-energy spectra of the AGATA demonstrator are shown. The top panel is related to the ^{80}Zr decay, while the bottom panel is related to the ^{81}Rb decay. The circles represent the transitions of the more populated residues.

A. Residual nuclei

When the excitation energy is higher than the particle binding energy, the compound nucleus decays emitting mainly particles until the excitation energy drops below the particle-separation energy, then it can decay only via γ-ray emission. The nuclei populated after the particle decay process are called residual nuclei. The γ rays associated with the low-energy transitions of the residual nuclei were detected using the AGATA demonstrator. These discrete transitions were used to identify the residual nuclei and to extract, using their intensities, the CN residual-nuclei population. In Fig. 11, the γ-ray spectra of the AGATA demonstrator are shown for both reactions. The main intense peaks were identified using the RADWARE archive [32]. The residual nuclei are populated with different yields, depending on the phase-space region they occupy.

To verify the agreement between the experimental data and the statistical-model calculations, we evaluated the variation of the residual-nuclei population as a function of F_γ and the γ-ray energy detected in HECTOR$^+$. In both cases, a variation is expected because of the change of the phase space available for particles emission.

The residual-nuclei population extracted using the AGATA demonstrator as a function of the γ-ray energy detected in HECTOR$^+$ is shown in Fig. 12. The experimental data were corrected by the AGATA demonstrator efficiency. The statistical-model calculations were performed using a Monte Carlo version of the CASCADE code. In Fig. 12, one can see that the ^{77}Rb residual nucleus (three protons emission) is strongly populated in coincidence with a high-energy γ ray (in the region of IVGDR); on the other hand, the ^{76}Kr residual nucleus (four protons emission) is mainly populated in coincidence

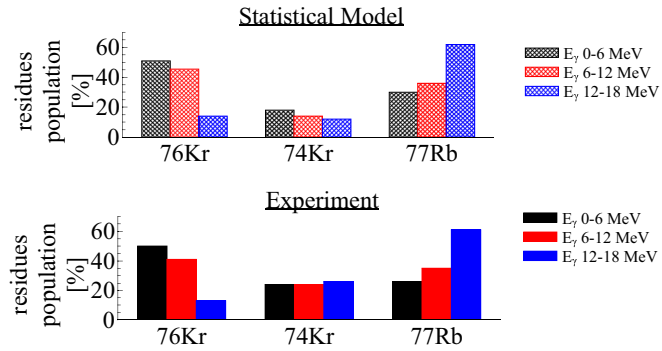

FIG. 12. Residual-nuclei population obtained from the analysis of the AGATA demonstrator spectrum as a function of the energy detected in the HECTOR$^+$ array. The experimental data were corrected with the AGATA demonstrator efficiency. The statistical-model calculations were performed using a Monte Carlo CASCADE code.

with low-energy γ rays. This fact reflects the population of two different regions of the phase space. In fact, gating on a high-energy γ ray, less phase-space is available for particles' emission and thus the population of the residual nucleus with less particles emitted is favored.

The variation of the residual-nuclei population as a function of the F_γ detected in HECTOR$^+$ and the AGATA demonstrator is shown in Fig. 13. The statistical-model data were obtained by folding the spin distributions with the $P(F_\gamma, M_\gamma)$ curves. From Fig. 14, one can see that the ^{77}Rb residual nucleus is more populated in high-F_γ events; on the other hand, the ^{76}Kr residual nucleus is more populated in low-F_γ events. Even in this case, the variation of the residual-nuclei population can be understood in terms of phase space: a higher F_γ corresponds to a selection of higher CN angular momentum and thus higher rotational energy. As a consequence, less energy is available for the particles' evaporation and the residual nucleus with less particles emitted is favored.

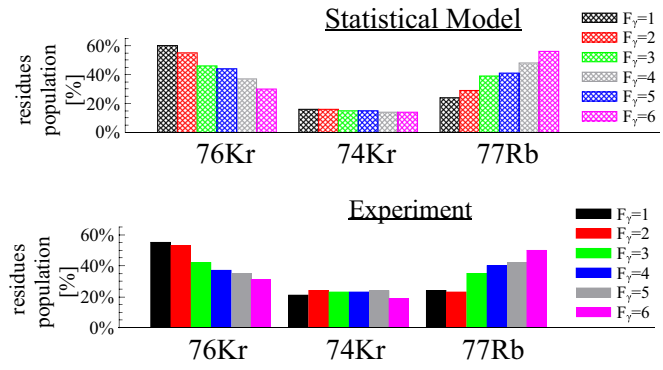

FIG. 13. Residual-nuclei population obtained from the analysis of the AGATA demonstrator spectrum as a function of the fold request. $F_\gamma = 1$ corresponds to one γ-ray detected in the AGATA demonstrator while $F_\gamma = 2,3,\ldots,6$ corresponds to $1,2,\ldots,5$ γ rays detected in the AGATA demonstrator and one in HECTOR$^+$, respectively. The statistical-model calculations were performed using a Monte Carlo CASCADE code.

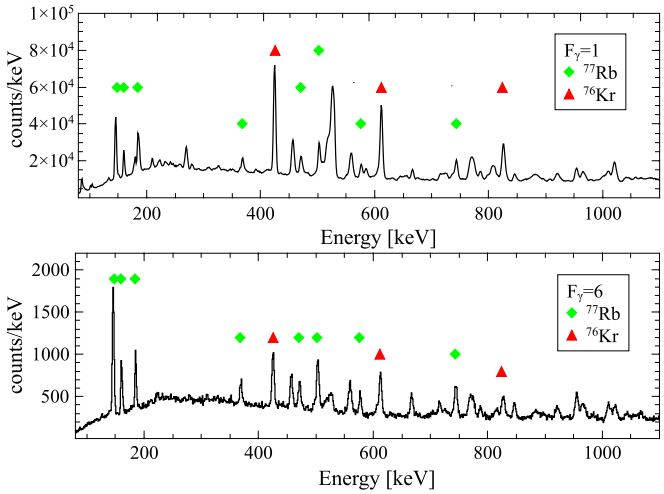

FIG. 14. Energy spectra of the AGATA demonstrator in the reaction ^{40}Ca + ^{40}Ca related to two different F_γ conditions: (top panel) $F_\gamma = 1$ spectrum (one γ ray detected in the AGATA demonstrator and zero in HECTOR$^+$, respectively); (bottom panel) $F_\gamma = 6$ spectrum (five γ- detected in the AGATA demonstrator and one in HECTOR$^+$, respectively).

In general, the three most strongly populated residual nuclei (^{76}Kr, ^{74}Kr, and ^{77}Rb) were found to be well reproduced by the statistical model. The same code was used for the analysis of the high-energy γ-ray spectra to deduce the GDR parameters and the isospin mixing.

IV. RESULTS

The statistical model provided the γ-ray spectrum of the CN, which was compared (after the folding with the detector response function and normalizing to the data at around 5 MeV) with the experimental data. The IVGDR parameters and the isospin mixing were derived from the best fit to the data in the region between 8 and 15 MeV. Due to the exponential nature of the spectra, the standard χ^2 is not a suitable quantity because of its weak sensitivity to the low-yield part of the spectrum. For this reason, the fit minimization was applied to a figure of merit (FOM) defined as

$$\mathrm{FOM} = \sum_{E=8\,\mathrm{MeV}}^{E=15\,\mathrm{MeV}} \frac{(Y_i - M_i)^2}{Y_i^2}, \tag{4}$$

where Y_i and M_i are the experimental and simulated counts per bin, respectively. Equation (4) was obtained by dividing the standard χ^2 over the number of counts for each bin. In this way, the sensitivity to the low-yield part of the spectrum is increased.

A. ^{81}Rb: Evolution of the GDR width

The width of a IVGDR built on an excited state increases with both the temperature and the angular momentum: the damping of the resonance feels the thermal-fluctuation effects in the excited nucleus. Using a critical-temperature-gluctuation model (CTFM) calculation [12,13], the temperature evolution of the IVGDR width can be parameterized as

$$\Gamma(T, J = 0, A) = c(A) \ln\left(\frac{T}{T_c}\right) + \Gamma_{\mathrm{int}}, \tag{5}$$

where $c(A) = 8.45 - A/50$, $T_c = 0.7 + 37.5/A$ is the critical temperature, and Γ_{int} is the intrinsic width of the GDR. Γ_{int} can be measured with a photoabsorption experiment. The angular-momentum dependence can be written as [12]

$$\frac{\Gamma(T, J, A)}{\Gamma(T, J = 0, A)} = [L(\xi = J/A^{5/6})]^{7T_c/(T+3.3T_c)}. \tag{6}$$

where $L(\xi) = 1 + 1.8/[1 + \exp^{(1.3-\xi)/0.2}]$. L is also called the reduced width, Γ_{red}, and it is equal to

$$\Gamma_{\mathrm{red}} = \left[\frac{\Gamma_{\mathrm{exp}}(T, J, A)}{\Gamma(T, J = 0, A)}\right]^{(T+3.3T_c)/7T_c}. \tag{7}$$

For ^{81}Rb the best-fitting values of the centroid, width, and strength of the IVGDR were found to be $E_{\mathrm{GDR}} = 16.4 \pm 0.2$ MeV, $\Gamma_{\mathrm{GDR}} = 7.0 \pm 0.2$ MeV, and $S_{\mathrm{GDR}} = 90 \pm 5\%$.

In Table III, both the experimental values and the theoretical calculations obtained with CTFM calculations are reported. The experimental values at $E^* = 83$ MeV were taken from Ref. [22]. In these calculations the intrinsic width of the GDR was taken from the photoabsorption experiment with $^{\mathrm{nat}}$Rb, $\Gamma_{\mathrm{int}} = 4.5$ MeV [33]. To compare in a linear scale experimental data and theoretical calculations, we used the quantity

$$F(E_\gamma) * Y_\gamma^{\mathrm{exp}}(E_\gamma)/Y_\gamma^{\mathrm{cal}}(E_\gamma), \tag{8}$$

where $F(E_\gamma)$ is the Lorentzian function that reproduces the IVGDR in the fitting procedure, $Y_\gamma^{\mathrm{exp}}(E_\gamma)$ is the measured γ-ray yield, and $Y_\gamma^{\mathrm{cal}}(E_\gamma)$ is the calculated γ-ray yield obtained by the CASCADE code. In Fig. 15 the comparison between the linearized experimental data and the theoretical curves is shown. The increase of the IVGDR width is well reproduced by the CTFM calculation and our values are in agreement with data obtained for nuclei in different mass regions (see Fig. 16).

TABLE III. Comparison between experimental data and theoretical calculations performed using a CTFM approach in the nucleus ^{81}Rb. The first row corresponds to a photoabsorption experiment, which allows one to obtain the intrinsic width of the IVGDR.

E^* (MeV)	J ($\hbar$)	T (MeV)	E_{GDR} (MeV)	Γ_{GDR} (MeV)	S_{GDR} (%)	$\Gamma_{\mathrm{GDR}}^{\mathrm{theory}}$ (MeV)
–	–	–	16.8	4.5	–	–
54	17	1.8	16.4 ± 0.2	7.0 ± 0.2	90 ± 5	7.7 ± 0.4
83	38	1.9	16.2 ± 0.2	10.8 ± 0.2	90 ± 3.5	11.3 ± 0.4

B. ^{80}Zr: Isospin mixing

The original version of the CASCADE code was first modified by Harakeh [20] and later on by the Washington University group [19], according to the formalism of Harney, Richter, and Weidenmüller [26].

Three features are relevant to correctly include isospin in the statistical-model code:

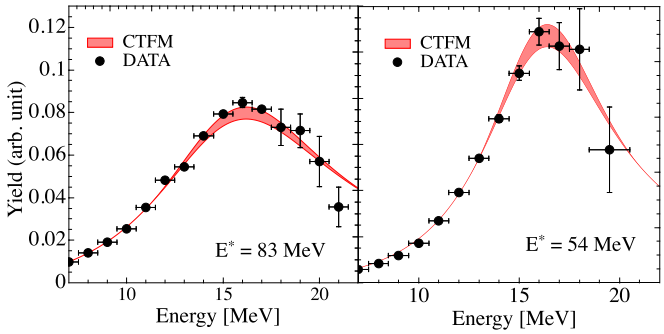

FIG. 15. Linearized γ-ray spectra compared with theoretical calculations performed using a CTFM calculation for the reaction ^{44}Ca +^{37}Cl. The red band reflects the uncertainty on the value of the temperature. In the left panel, the experimental data at $E^* = 83$ MeV obtained in Ref. [22] are shown. In the right panel, the data at $E^* = 54$ MeV obtained in our experiment are shown.

(i) the population cross section matrices and level densities are labeled with the quantum number for isospin (in addition to excitation energy, angular momentum, and parity);
(ii) the states with different isospin are mixed before any type of decay (according to the CN hypothesis);
(iii) the transmission coefficients are multiplied by isospin Clebsch-Gordan coefficients.

In the statistical model two classes of isospin are considered: $I_< = I_z$ and $I_> = I_z + 1$. The initial compound nucleus is populated in the state $I_<$ according to the isospin conservation in nuclear reactions. The state $I_>$ is populated thanks to the mixing according to the following equations:

$$\begin{aligned}\widehat{\sigma_<} &= (1-\alpha_<^2)\sigma_< + \alpha_>^2\sigma_>,\\ \widehat{\sigma_>} &= (1-\alpha_>^2)\sigma_> + \alpha_<^2\sigma_<,\end{aligned} \tag{9}$$

where $\sigma_<$ ($\sigma_>$) is the cross section to form the CN in the state $I_<$ ($I_>$) without the mixing. $\widehat{\sigma_<}$ ($\widehat{\sigma_>}$) is the mixed cross section. $\alpha_<^2$ ($\alpha_>^2$) is the probability that a fraction of state $I_<$ ($I_>$) mixes to a state $I_>$ ($I_<$). These quantities are defined in the statistical model according to the following equations:

$$\begin{aligned}\alpha_<^2 &= \frac{\Gamma_<^{\downarrow}/\Gamma_<}{1+\Gamma_<^{\downarrow}/\Gamma_< + \Gamma_>^{\downarrow}/\Gamma_>},\\ \alpha_>^2 &= \frac{\Gamma_>^{\downarrow}/\Gamma_>}{1+\Gamma_>^{\downarrow}/\Gamma_> + \Gamma_<^{\downarrow}/\Gamma_<},\end{aligned} \tag{10}$$

where $\Gamma_{>(<)}$ is the total decay width of the states $I_{>(<)}$. $\Gamma_<^{\downarrow}$ and $\Gamma_>^{\downarrow}$ are the Coulomb spreading width of the two states, which can be written as

$$\begin{aligned}\Gamma_>^{\downarrow} &= 2\pi\overline{|\langle I_<|H_c|I_>\rangle|^2}\rho[I_<],\\ \Gamma_<^{\downarrow} &= 2\pi\overline{|\langle I_>|H_c|I_<\rangle|^2}\rho[I_>],\end{aligned} \tag{11}$$

where H_c is the isovector part of the Coulomb interaction and $\rho[I_<]$ and $\rho[I_>]$ are the level densities of the two types of states. It is worth noting that for small mixing, Eq. (11) is reduced to $\Gamma_<^{\downarrow}/\Gamma_< = \tau_{CN}/\tau_{mix}$, confirming the Wilkinson's hypothesis that the mixing at finite excitation energy depends only on the competition between the mixing and the CN decay. For intermediate value of the mixing, it is necessary to include the terms in the denominator $\Gamma_{<(>)}^{\downarrow}/\Gamma_{<(>)}$, which takes into account also the probability that $I_{<(>)}$ states mix back to $I_{>(<)}$. This model assumes that the two classes of states are centered at the same excitation energy and, consequently, the relation

$$\Gamma_<^{\downarrow} = \frac{\rho[I_>]}{\rho[I_<]}\Gamma_>^{\downarrow} \tag{12}$$

is valid. To extract the isospin-mixing probability in ^{80}Zr the Coulomb spreading width was treated as the only free parameter to fit the ^{80}Zr data, all the other parameters were fixed from ^{81}Rb analysis. The best fit of the ^{80}Zr data was obtained with a Coulomb spreading width equal to $\Gamma_C^{\downarrow} = \Gamma_>^{\downarrow} = 12 \pm 3$ keV.

The value of the Coulomb spreading width is in good agreement with that found in Ref. [22] $\Gamma_C^{\downarrow} = 10 \pm 3$ keV. It means that the Coulomb spreading width is an intrinsic property of the system and it does not strongly depend on its excitation energy.

In addition, our value is also consistent with the one found in ^{80}Se studying the spreading width of the isobaric analog state (IAS) $\Gamma_{IAS}^{\downarrow} = 9.9 \pm 0.6$ keV [34]. This result supports the idea that the Coulomb spreading width of the CN and the IAS are strongly connected because both quantities originate from the isospin-mixing phenomenon.

In Fig. 17, our value of $\Gamma_C^{\downarrow}$ (blue circle) is compared with the ones available in the literature (see Ref. [26] and references therein). Our datum is in good agreement with the experimental trend: the $\Gamma_C^{\downarrow}$ remains rather constant until mass A $\approx$ 120. In addition, the experimental data obtained with the study of the statistical decay of the CN are in good agreement with the values obtained studying the IAS.

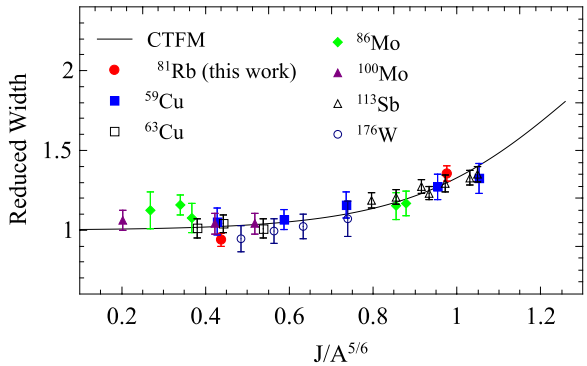

FIG. 16. GDR reduced-width evolution as a function of the parameter ξ for different nuclei. The black curve represents the function $L(\xi)$ in the CTFM. The experimental data were taken from Ref. [12] and references therein.

V. SUMMARY AND CONCLUSIONS

The IVGDR γ decay was measured in the compound nuclei ^{80}Zr and ^{81}Rb at $E^* = 54$ MeV and $\langle J\rangle \approx 20\ \hbar$.

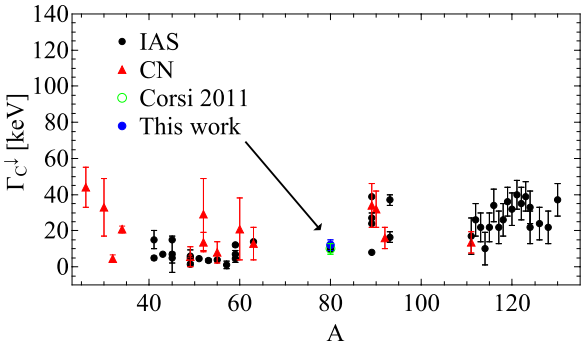

FIG. 17. Values of the Coulomb spreading width obtained in the IAS (black dots) data and data from the CN (red triangles) [26]. The arrow points to the value obtained in our work (blue circle), overlapping with the value obtained in Corsi 2011 [22] (empty green dot).

The analysis of the high-energy spectra was performed using a statistical-model approach. The measurement of the low-energy transitions with the AGATA demonstrator provided a stringent test to the CN decay predicted by the statistical model. A good agreement between experimental data and calculations was found.

The measured IVGDR width in ^{81}Rb was found to be significantly smaller than the one in Ref. [22] at higher excitation energy and angular momentum. This result is well reproduced by CTFM calculations. These calculations are based on the assumption that the intrinsic width of the resonance does not depend on the excitation energy of the system.

The Coulomb spreading width obtained in the nucleus ^{80}Zr is in agreement with the one found at higher excitation energy in Ref. [22] and also with the one found in ^{80}Se by studying the IAS width [34]. This implies two facts: (i) the Coulomb spreading width does not change with the excitation energy; and (ii) the Coulomb spreading widths obtained in the CN are the same as the ones obtained in the IAS, in accordance with the fact that they originate from the same isospin-violating force.

In conclusion, in this work we have shown the importance of the study of the IVGDR to obtain information on basic quantities in nuclear structure at finite excitation energy, such as the shape evolution in hot nuclei and the isospin symmetry. Although the isospin-mixing probability and the IVGDR width change with the excitation energy of the system, we have found, in the same system, that the intrinsic quantities $\Gamma_C^{\downarrow}$ and Γ_{int} remain constant independent of the excitation energy of the nucleus. It will be interesting to further address these questions far from the stability when second-generation radioactive beams will allow us to reach new regions in the nuclear chart.

ACKNOWLEDGMENTS

This work was supported by the Polish National Science Centre Grants No. 2015/17/B/ST2/01534 and No. 2015/17/N/ST2/04034.

[1] M. N. Harakeh and A. van der Woude, *Giant Resonances: Fundamental High-Frequency Modes of Nuclear Excitation* (Oxford University, London, 2001).
[2] P. F. Bortignon, A. Bracco, and R. A. Broglia, *Giant Resonances: Nuclear Structure at Finite Temperature*, Contemporary Concepts in Physics, Vol. 10 (Harwood Academic, Chur, Switzerland, 1998).
[3] J. J. Gaardhøje, Ann. Rev. Nucl. Part. Sci. **42**, 483 (1992).
[4] K. Snover, Ann. Rev. Nucl. Part. Sci. **36**, 545 (1986).
[5] D. M. Brink, Ph.D. thesis, Oxford University, 1955.
[6] P. Axel, Phys. Rev. **126**, 671 (1962).
[7] A. Bracco, F. Camera, M. Mattiuzzi, B. Million, M. Pignanelli, J. J. Gaardhøje, A. Maj, T. Ramsøy, T. Tveter, and Z. Źelazny, Phys. Rev. Lett. **74**, 3748 (1995).
[8] O. Wieland *et al.*, Phys. Rev. Lett. **97**, 012501 (2006).
[9] M. Mattiuzzi *et al.*, Nucl. Phys. A **612**, 262 (1997).
[10] D. Kusnezov, Y. Alhassid, and K. A. Snover, Phys. Rev. Lett. **81**, 542 (1998).
[11] D. Kusnezov and W. E. Ormand, Phys. Rev. Lett. **90**, 042501 (2003).
[12] D. Pandit, S. Mukhopadhyay, S. Pal, A. De, and S. R. Banerjee, Phys. Lett. B **713**, 434 (2012).
[13] D. Pandit, S. Bhattacharya, B. Dey, D. Mondal, S. Mukhopadhyay, S. Pal, A. De, and S. R. Banerjee, Phys. Rev. C **88**, 054327 (2013).
[14] M. Ciemała *et al.*, Phys. Rev. C **91**, 054313 (2015).
[15] D. H. Wilkinson, *Isospin in Nuclear Physics* (North-Holland, Amsterdam, 1969).
[16] G. Colò, M. A. Nagarajan, P. Van Isacker, and A. Vitturi, Phys. Rev. C **52**, R1175 (1995).
[17] H. Sagawa, P. F. Bortignon, and G. Colò, Phys. Lett. B **444**, 1 (1998).
[18] E. Farnea *et al.*, Phys. Lett. B **551**, 56 (2003).
[19] J. A. Behr, K. A. Snover, C. A. Gossett, M. Kicińska-Habior, J. H. Gundlach, Z. M. Drebi, M. S. Kaplan, and D. P. Wells, Phys. Rev. Lett. **70**, 3201 (1993).
[20] M. N. Harakeh *et al.*, Phys. Lett. B **176**, 297 (1986).
[21] M. Kicińska-Habior *et al.*, Nucl. Phys. A **731**, 138 (2004).
[22] A. Corsi *et al.*, Phys. Rev. C. **84**, 041304(R) (2011).
[23] S. Ceruti *et al.*, Phys. Rev. Lett. **115**, 222502 (2015).
[24] D. H. Wilkinson, Philos. Mag. **1**, 379 (1956).
[25] H. Morinaga, Phys. Rev. **97**, 444 (1955).
[26] H. L. Harney, A. Ritcher, and H. A. Weidenmüller, Rev. Mod. Phys. **58**, 607 (1986).
[27] AGATA Collaboration, Nucl. Instrum. Methods Phys. Res., Sect. A **668**, 26 (2012).
[28] A. Giaz *et al.*, Nucl. Instrum. Methods Phys. Res., Sect. A **729**, 910 (2013).
[29] F. Pühlhofer, Nucl. Phys. A **280**, 267 (1977).
[30] S. Agostinelli *et al.*, Nucl. Instrum. Methods Phys. Res., Sect. A **506**, 250 (2003).
[31] A. Maj *et al.*, Nucl. Phys. A **571**, 185 (1994).
[32] D. C. Radford, Nucl. Instrum. Methods Phys. Res., Sect. A **361**, 297 (1995).
[33] B. L. Berman and S. C. Fultz, Rev. Mod. Phys. **47**, 713 (1975).
[34] S. Kailas *et al.*, Nucl. Phys. A **315**, 157 (1979).